EXPERIMENTAL STUDY ON THE DYNAMIC STRESS-STRAIN BEHAVIOR OF EXPANDED POLYSTYRENE GEOFOAM USING CYCLIC TRIAXIAL TESTS

by

Benjamin A. Erickson

A thesis submitted to the faculty of
The University of Utah
in partial fulfillment of the requirements for the degree of

Master of Science

in

Geological Engineering

Department of Geology and Geophysics

The University of Utah

December 2011

The University of Utah Graduate School

STATEMENT OF THESIS APPROVAL

The thesis of **Benjamin A. Erickson**

has been approved by the following supervisory committee members:

Aurelian C. Trandafir	, Chair	**10/27/2011** Date Approved
Steven F. Bartlett	, Member	**10/27/2011** Date Approved
Ronald L. Bruhn	, Member	**10/27/2011** Date Approved

and by **D. Kip Solomon** , Chair of

the Department of **Geology & Geophysics**

and by Charles A. Wight, Dean of The Graduate School.

ABSTRACT

Dynamic testing of expanded polystyrene (EPS) results in behavior alterations when certain testing criteria are modified. Triaxial testing affirms the behavior of EPS geofoam under axial compression tests related to a seismic compressible inclusion application. An evaluation of initial static deviator stress, load frequency of deviator stress amplitudes, and the effect of static confining stress of EPS geofoam dynamic response are performed. The behavior of viscoelastic and visco-elasto-plastic are compared through the use of cyclic compression tests. Comparative measurements used in supporting behavior change were: Young's modulus, damping ratio, cyclic deviator stress, and plastic axial strains. The resulting data is interpreted through data charts and data trends. Comparative conclusions show significant behavior changes to EPS geofoam when frequency and confining stress influential effects are observed.

To my inspirational and loving wife

TABLE OF CONTENTS

ACKNOWLEDGMENTS

The opportunity of conducting this research would not have been possible without the help of many people and organizations. I wish to first acknowledge the efforts of Dr. Aurelian C. Trandafir for being an outstanding advisor for this work and a wonderful mentor throughout my graduate studies. I also offer my gratitude to Dr. Ronald L. Bruhn and Dr. Steven F. Bartlett, members of my supervisory committee, providing expertise and wisdom regarding this study. This work was made possible through support of the National Science Foundation under Grant No. CMMI-0926042 and ACH Foam Technologies LLC, Salt Lake City, Utah providing the EPS geofoam specimens.

I also wish to express my great appreciation and gratitude to my friends and family who encouraged and supported me through this research.

INTRODUCTION

For the past 40 years the petroleum based product, expanded polystyrene (EPS) geofoam (Figure 1), has been an integral part of geotechnical applications. Geofoam was originally used by the Norwegian Road Research Laboratory for soil replacements fill, which employs the fill light weight function (Frydenlund and Aabøe, 2001). In this capacity, geofoam prevents soil subsidence and expedites soil consolidation wait times. Several studies have examined the behavior of geofoam and produced results beneficial in the evolution of its application (Horvath, 1995; Negussey, 1997; Bathurst et al, 2006; Hazarika, 2006; Wong and Leo, 2006). Roadways (including railways and highways), embankments (Horvath, 1995; EPS 96; EPS 2001; EPS 2011), pipelines (Choo et al, 2007) and building construction (Ikizler et al, 2007) have been made possible where native conditions prevented these projects due to the occurrence of soft and highly compressible soils. Figures 2 and 3 illustrate diagram examples the light weight fill function of the geofoam for embankments as well as backfill applications. Figure 4 is current construction project in Salt Lake City, Utah, for the Utah Transit Authority Trax project where blocks of geofoam are used as light weight fill for an approaching fill to a viaduct crossing North Temple Street for vehicular and light rail traffic.

Additional research has proven the effectiveness of geofoam in reducing the lateral earth pressures (Horvath, 1996) and seismic vibration insulation (Murillo et al, 2009; Zarnani and Bathurst, 2009). From the additional research for seismic isolation and

Figure 1: A 10 cm diameter 20 cm height (2:1 ratio) cylindrical sample of EPS geofoam.

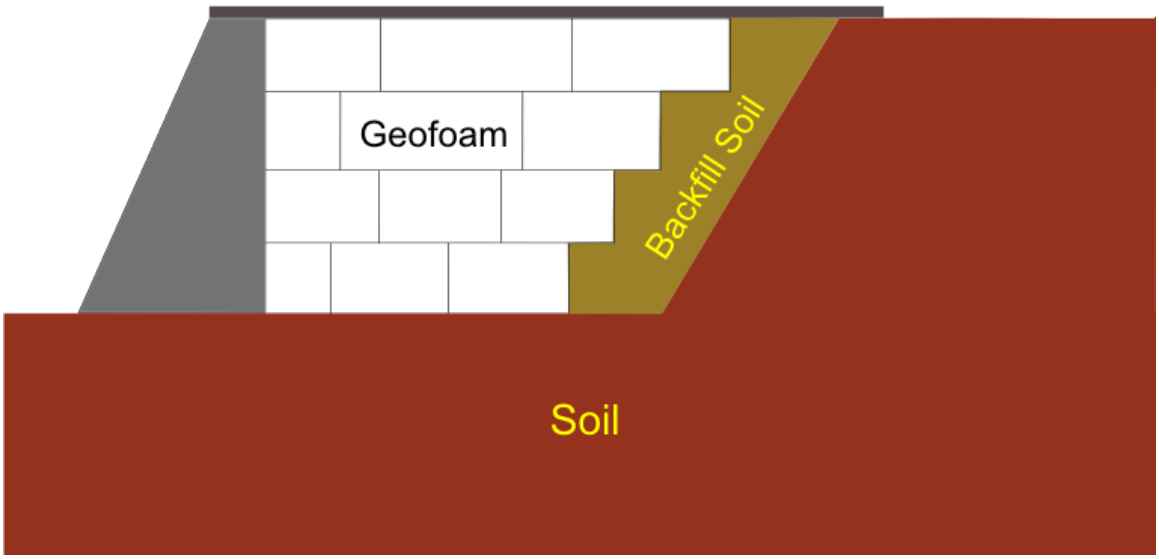

Figure 2: EPS back fill diagram implementing EPS geofoam for soil replacement.

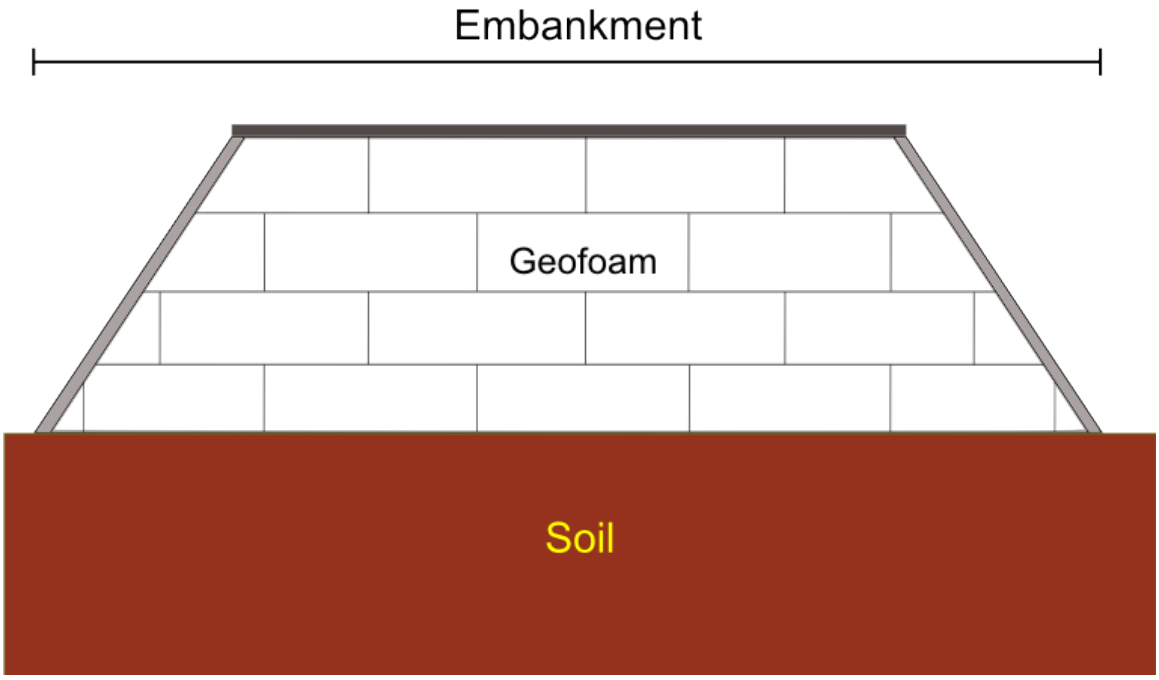

Figure 3: EPS geofoam application diagram for an embankment soil replacement.

Figure 4: Recent viaduct construction project in Salt Lake City, Utah implementing EPS geofoam as soil replacement.

earth pressure reduction, construction designs have evolved to include geofoam (Bathurst et al, 2006; Zarnani and Bathurst, 2008). Figures 5 and 6 demonstrate the use of geofoam as compressible inclusions within the design of rigid walls and a buried pipe or culvert (Choo et al, 2007).

The reason why expanded polystyrene is an integral part of the aforementioned construction projects is due to its physical properties. Being ultra lightweight with a density that is approximately $1/100^{th}$ of sand (Lin et al, 2010; Osborn, 2004), it provides a replacement for weak soils preventing settlement; a water proof material allowing for placement below the water table; potential lower design costs and efficiency in installation provides additional economic advantages for planned construction projects. Due to its moderately high compressibility, it can be used as a compressible inclusion to provide a decrease soil lateral pressures (Horvath, 1996); due to its high compressibility, EPS provides a decrease in high lateral earth pressures against retaining walls under both static and dynamic conditions (Murillo et al, 2009; Trandafir et al, 2010b).

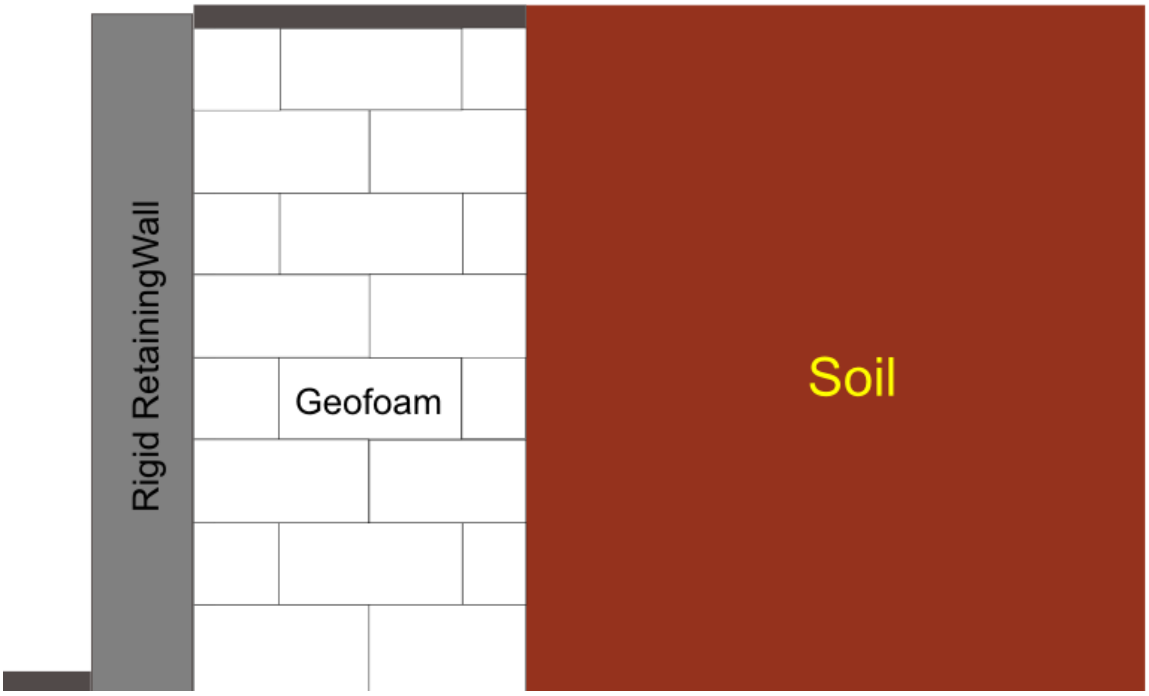

Figure 5: EPS geofoam applied as a compressible inclusion between a rigid retaining wall and retained soil.

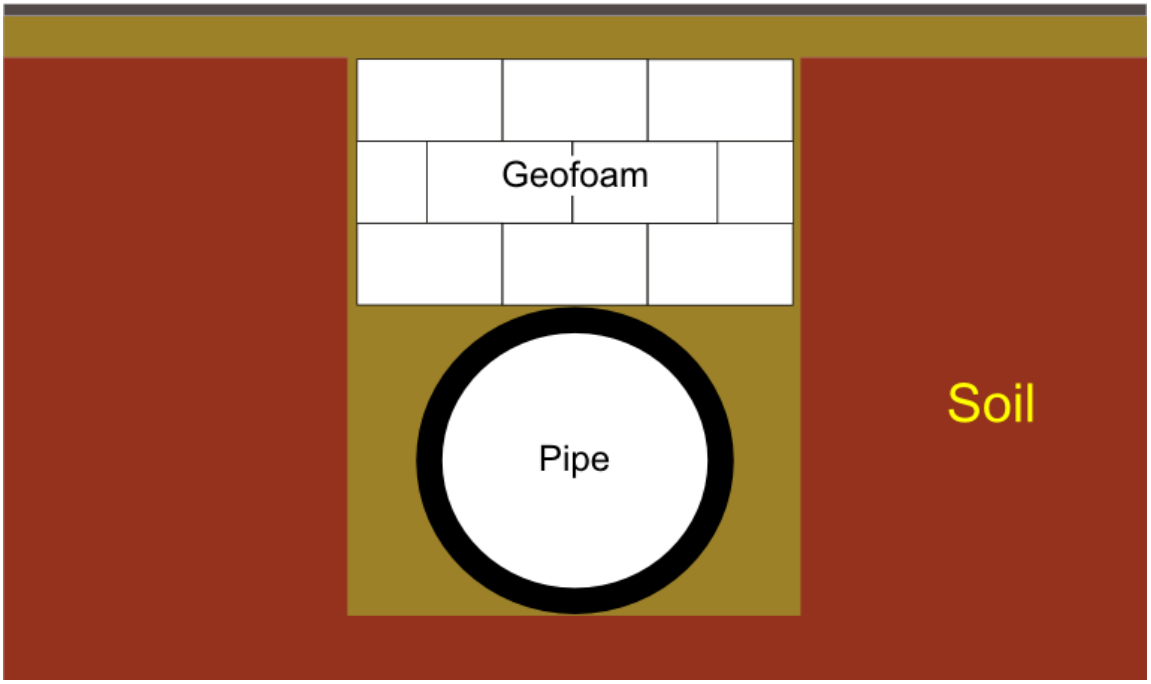

Figure 6: EPS geofoam implemented as a compressible inclusion between the ground surface and a pipe or culvert.

OBJECTIVES

In the context of the compressible inclusion function of geofoam, the present investigation focuses on a better understating of the dynamic behavior of this material which is crucial in optimizing the seismic buffer function of geofoam in retaining wall applications. Specifically, this study aims at examining how various initial (static) stress conditions acting on geofoam as well as various amplitudes and frequencies of cyclic loading influence the dynamic response of the material. In order to accomplish this, an experimental study based on cyclic axial compression test has been undertaken. The specific objectives of the axial compression tests as related to the seismic compressible inclusion application are outlined as follows:

1) The effect of initial (static) deviator stress on the cyclic stress-strain behavior of geofoam. This set of experiments will provide insight into the effect of the various static lateral earth pressures (acting against the geofoam panel behind the retaining wall) on the dynamic behavior of EPS geofoam.

2) The effect of loading frequency and cyclic deviator stress amplitudes on the dynamic response of geofoam.

3) The effect of the static confining stress of geofoam dynamic response. The set of experiments in the confining environment will offer insight for lateral earth pressures acting on geofoam within a confined environment under dynamic conditions.

EXPERIMENTAL SETUP

Testing material

EPS geofoam is comprised of small beads of solid petroleum based styrene (i,e., plastic). These beads are prepared for polymerization using alkanes (i.e., ethane, pentane, etc.) in a high heat and pressure environment. The expanded polystyrene formation requires a long molecule chain, which comes from slow polymerization. Quick polymerization will result in short molecule chains which will result in a weaker material (Lin et al., 2010).

The test specimens were provided by ACH Foam Technologies LLC, Salt Lake City, Utah. The geofoam tested densities of 15 kg/m^3, 19 kg/m^3 and 25 kg/m^3 denoted as EPS15, EPS19 and EPS25, respectively. Tested sample dimensions were 100 mm diameter with a height to diameter ratio of 2:1.

Test procedure

The testing for this study followed the procedure used to determine the cyclic behavior of geofoam as outlined by A. C. Trandafir (2010a) for stress-controlled uniaxial cyclic tests. The EPS geofoam specimens were tested using state-of-the-art, fully automated microprocessor-controlled cyclic triaxial equipment manufactured by Geocomp Corporation (Boxborough, MA). The triaxial equipment (Figure 7) was

available in the Geology and Geophysics Department at the University of Utah located in Salt Lake City, Utah for the purpose of this study.

The triaxial system is capable of reproducing all of the necessary cyclic loads required for the anticipated tests. In addition, the counterpart Geocomp software provides fully automated triaxial tests, analysis and stores data of the experiment.

The testing program included triaxial and uniaxial tests. For the cyclic uniaxial compression test an initial static deviator stress was applied on the specimen prior to the cyclic loading of the testing process (Figure 8). The static stress magnitude was within the pseudo-elastic range (Athansopoulos, 1999) of the geofoam to ensure no permanent deformation would occur. The cyclic loading phase started after the creep of the material under the static load has ceased. Material creep duration varied on applied magnitude of static deviator stress. Generally creep time ranged from 1 minute to 20 minutes.

The applied static deviator stress has a greater magnitude than the amplitude of the cyclic deviator stress to maintain the dynamic deviator stresses in the compression range during the unloading part of the cycle. For a given static deviator stress, various cyclic deviator stresses were applied at the various loading frequencies. For example, a set of tests with a static deviator stress of 30 kPa would be subjected to increasing amplitude deviator stresses of 2, 5, 10, 15, 20, 25 and 28 kPa, with each value constituting one test maintaining the same sample within the viscoelastic behavior range. Samples were changed once visco-elasto-plastic yielding was achieved.

In order to study the frequency effects, tests were conducted comparing frequencies of 0.5, 1.5 and 3.0 Hz. The number of cycles used was determined by the viscoelastic or visco-elasto-plastic responses of the material. For tests associated with

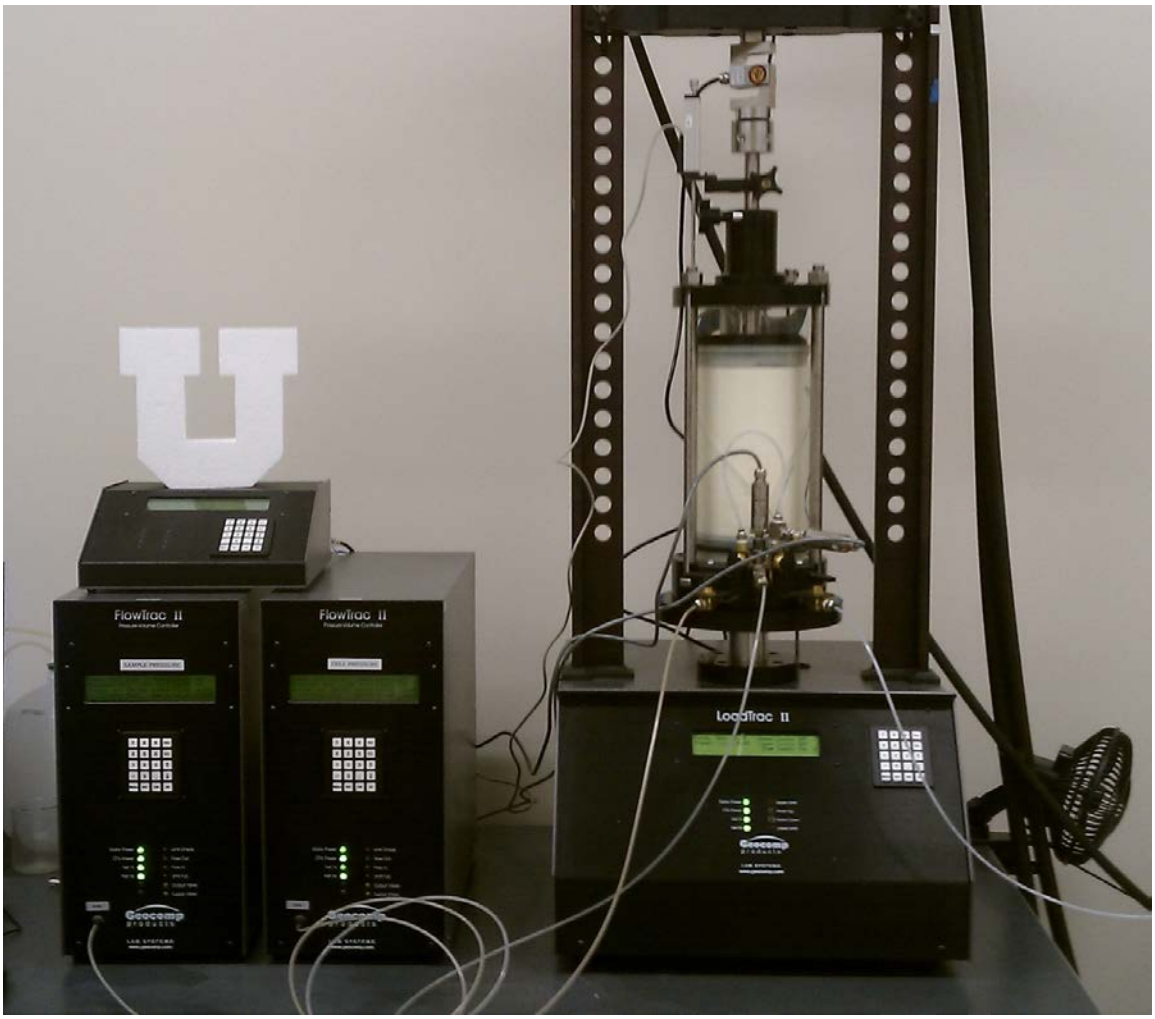

Figure 7: Geocomp cyclic triaxial equipment. 100 mm diameter sample of EPS geofoam prepared in triaxial equipment prepared for testing.

viscoelastic responses, a lower number of cycles would be used (i.e., $N = 30$). For visco-elasto-plastic responses, a higher number of cycles was applied (i.e., N = 100-300) in order to better characterize the plastic yielding behavior of the material.

The triaxial tests were performed for a loading frequency f = 1.5 Hz. Various isotropic confining stress states were considered with varying the cyclic deviator stress amplitude for a given confining stress, in a similar manner as uniaxial tests. Associated viscoelastic responses will use a lower cycle number while visco-elasto-plastic behavior will result in a higher cycle number.

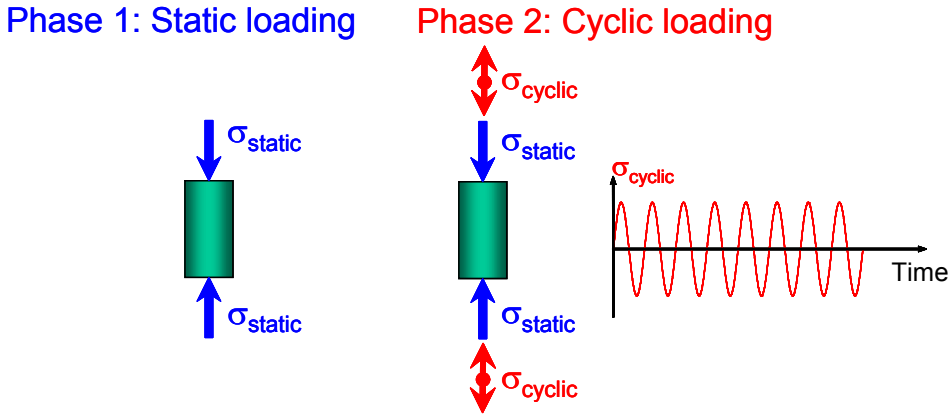

Figure 8: Testing procedure for the cyclic uniaxial test.

UNIAXIAL AND TRIAXIAL TESTING

Uniaxial compression tests consist of zero confining stress ($\sigma_c = 0$). As previously mentioned, for the cyclic loading tests, an initial static deviator stress (σ_{ds}) was applied with a magnitude greater than the range of the cyclic deviator stress ($\Delta\sigma_{dc}$) and was maintained until material creep ceased. This was applied to the sample prior to the cyclic loading phase of the test. The static minor and major principal stresses in the uniaxial tests are identified as $\sigma_{3s} = \sigma_c = 0$ and $\sigma_{1s} = \sigma_{ds}$, respectively. Figure 9 illustrates a conceptual model of EPS geofoam as a seismic buffer inclusion. The geofoam sample for cyclic uniaxial compression tests is considered a small element of the geofoam inclusion between the rigid wall and retained soil. For cyclic uniaxial compression tests, the confining pressure is considered zero.

The triaxial compression test involved a static initial isotropic stress state applied to the sample corresponding to the confining stress equivalent applied to the sample prior to the cyclic loading phase. The static minor and major principal stresses for these tests are identified as $\sigma_{1s} = \sigma_{3s} = \sigma_c$, respectively. As with the cyclic uniaxial compression tests, Figure 10 illustrates the seismic buffer concept regarding a buried structure with EPS geofoam inclusions between the structure and the surrounding soil. Due to the surrounding soil, the model's confining stress is greater than zero as translated by the cyclic triaxial compression test simulating a seismic event on the geofoam sample.

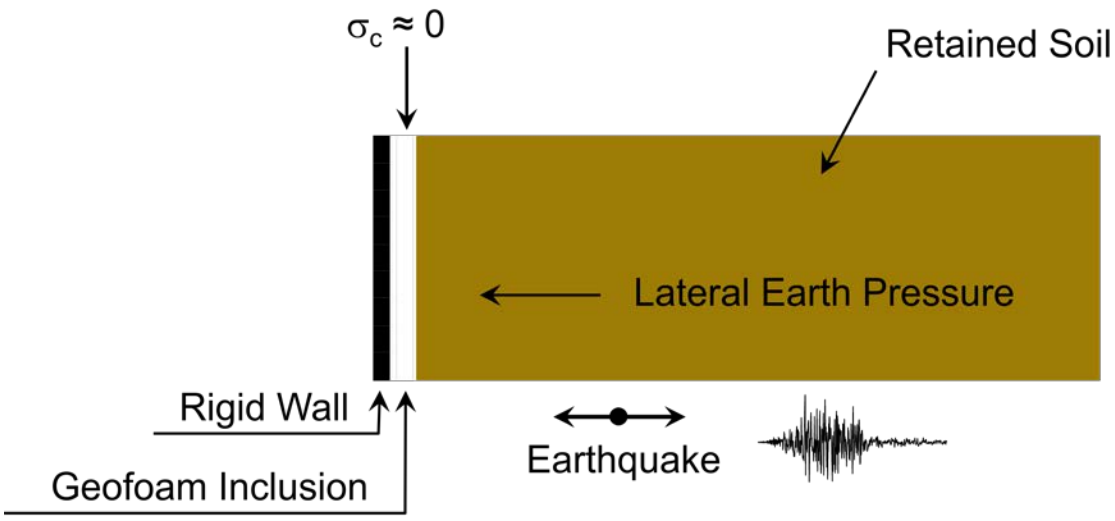

Figure 9: Representative element test of the seismic buffer concept. Cyclic uniaxial compression test ($\sigma_c = 0$).

The maximum static deviator stress applied in the uniaxial test corresponded to axial strains not greater than 1%, which is EPS geofoam elastic limit (Stark, 2004). The parameters of the cyclic loading were frequency of cyclic loading, amplitude of cyclic deviator stress and the number of loading cycles applied. For the uniaxial tests a range of 0.5-3.0 Hz was used, while triaxial tests used a 1.5 Hz cyclic loading frequency. The cyclic deviator stress, as previously discussed, was incrementally increased for a given value of the applied static deviator stress but no greater than the static deviator stress ($\sigma_{ds} > \Delta\sigma_d$). The parameter, $\sigma_{ds} > \Delta\sigma_{dc}$, required a constant interface connection between the sample and the testing equipment. This continuous interface connection ensures accurate measured responses of the material under cyclic loading. For the test sets the applied loading cycles ranged from 30 for tests characterizing viscoelastic response (i.e., σ_{ds} and $\Delta\sigma_{dc} < 1\%$ axial strain) to 300 for tests exhibiting visco-elasto-plastic behavior of EPS geofoam.

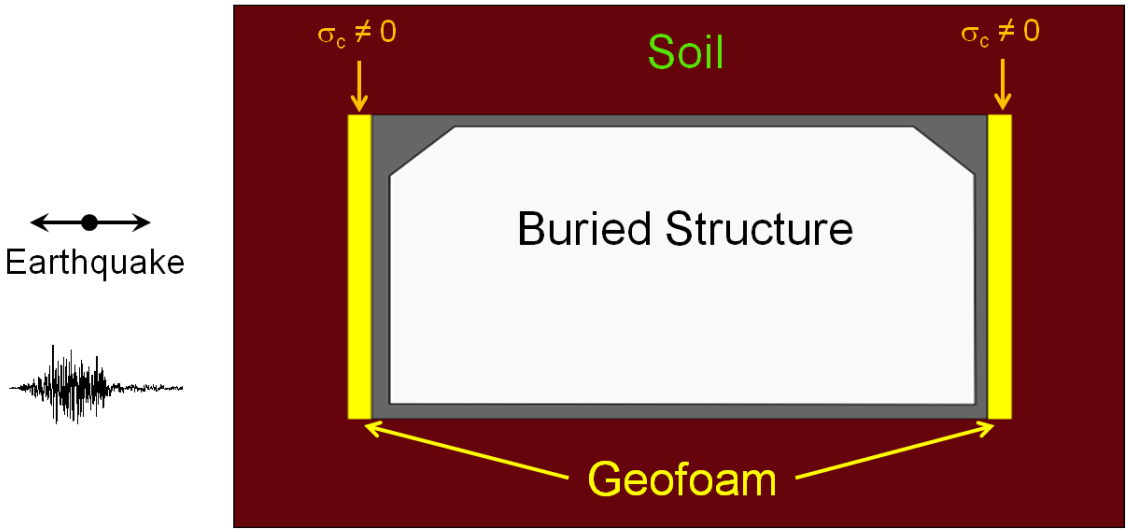

Figure 10: Seismic buffer concept - rigid walls of buried structure. Representative element test: Cyclic compression ($\sigma_c \neq 0$).

Viscoelastic results

The viscoelastic response of geofoam was examined using Young's modulus and damping ratio corresponding to various axial strain amplitudes. Figure 11 is an idealized hysteresis loop representation of the Young's modulus (E) and the viscoelastic behavior of EPS geofoam. The y axis is the cyclic deviator stress (σ_{dc}) and the x axis is the axial strain (ε_a). Where W_d and W_s are the energy values required for the damping ratio (D) calculations. The resulting damping ratio value is valid for one complete hysteresis loop.

The damping ratio describes the material's ability to dissipate energy by viscous mechanisms, where dissipated energy is per unit volume of one hysteresis loop (W_d). The Young's modulus (E) is determined by the secant modulus defined by the slope of the line through the origin and the initiation point of load reversal. The stored energy (W_s), as depicted in Figure 11, is the same as an elastic material resulting in the same E value for the material.

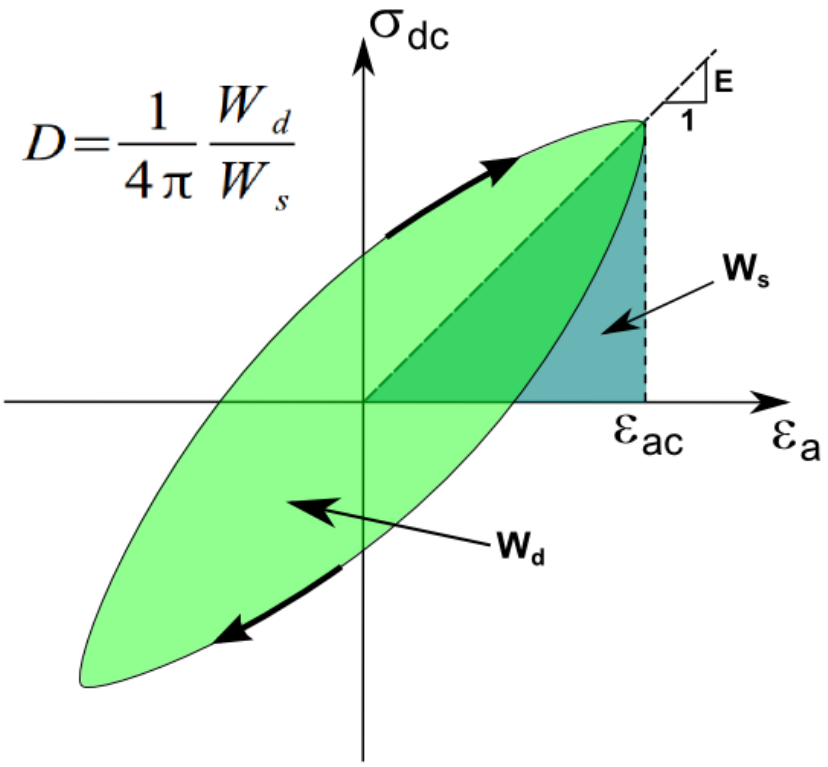

Figure 11: Hysteresis loop diagram for a viscoelastic material describing the Young's modulus (E), and energy values (Wd, Ws) in the determination of the damping ratio (D) for a material.

In addition to the calculation of the damping ratio, the normalized modulus (E/E_0) degradation curve can be determined. The E/E_0 degradation curve is obtained through the exponential regression best fit line of the experimental E/E_0 values. These values are related by the following equations obtained through the regression analysis of the data:

$$\frac{E}{E_0} = \alpha\, e^{\beta \varepsilon_{ac}} \tag{1}$$

where cyclic axial strain amplitude % is ε_{ac} and the regression parameters α and β are related with the density (ρ) and the static deviator stress (σ_{ds}) of geofoam. The associated equations of α and β are as follows

$$\alpha = \rho^{0.04}(0.9348 - 0.0009\sigma_{ds}) \quad (2)$$

$$\beta = -0.1457\frac{\rho^{2.5}}{\sigma_{ds}^{1.9699}} \quad (3)$$

with ρ and σ_{ds} values are kg/m^3 and kPa with the R^2 values of 0.9097 for α and 0.9299 for β respectively.

To illustrate the application of these formulas, Figures 12-14 offer comparative results predicted by formulas (1), (2) and (3) compared to measured regression lines of data from performed tests.

Figures 12-14 show an apparent sensitivity in the normalized modulus curve to the static deviator stress (σ_{ds}) by means of a more pronounced reduction of the normalized modulus for smaller static deviator stress values. The reduction of the normalized modulus appears to be related to material fabric alteration, due to material creep prior to cyclic loading. The creep appears to alter the material properties creating a stiffening effect which increases as the static deviator stress increases providing more resistance to loading for the material. Moreover, further analysis of martial creep need to be evaluated to offer a definitive conclusion for EPS geofoam and its effects under static deviator stress.

However, for the measured damping ratio (*D*) there is no apparent influence from the changing σ_{ds} values as well as no relationship with cyclic axial strain amplitudes with a wide data scattering from the regression line. As a trend, *D* shows a slight decrease as the cyclic axial strain increases.

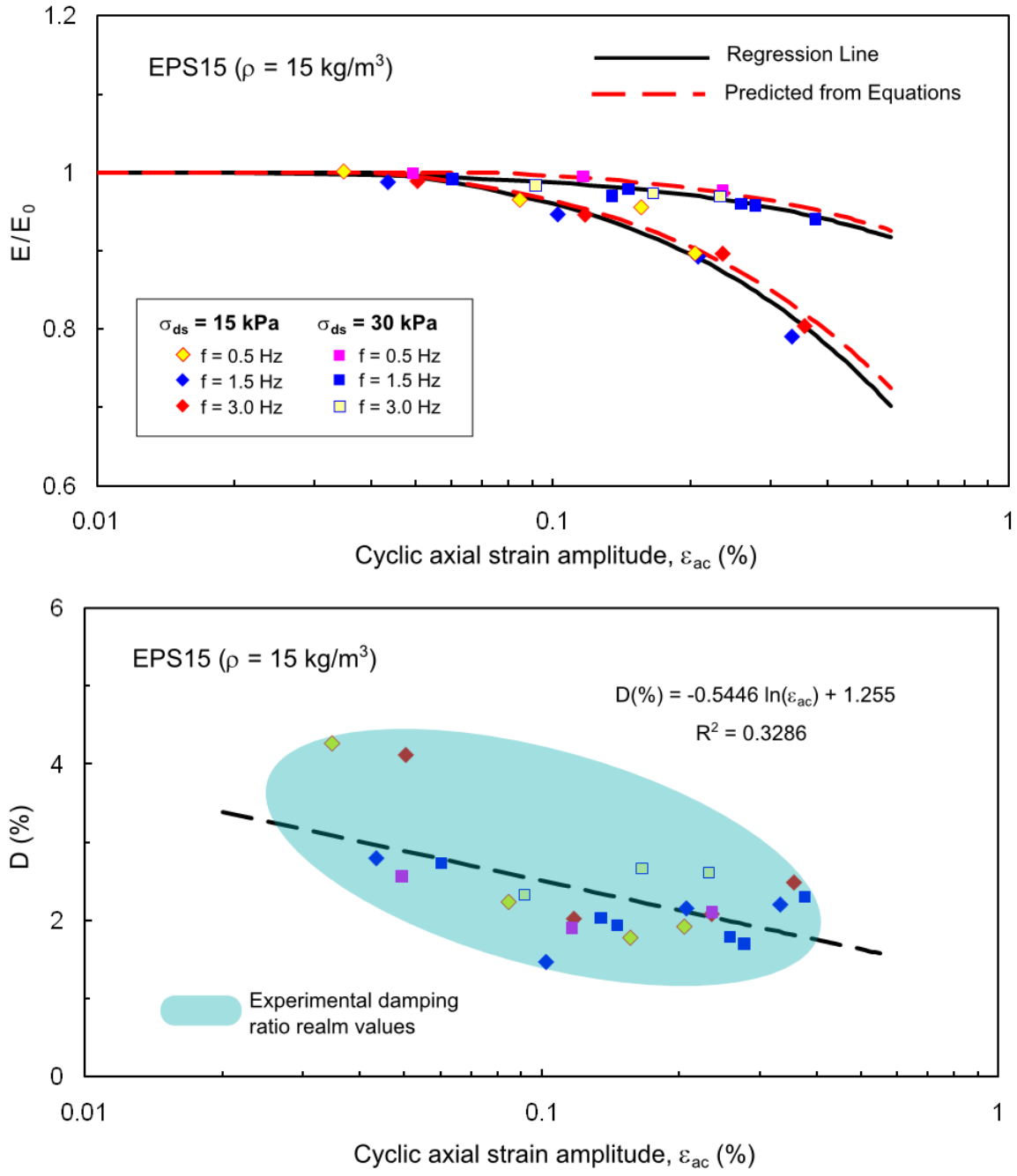

Figure 12: The normalized Young's modulus (E/E_0) and damping ratio (D) of EPS15 geofoam vs cyclic axial strain amplitude (ε_{ac}) for various static deviator stress (σ_{ds}) and loading frequencies

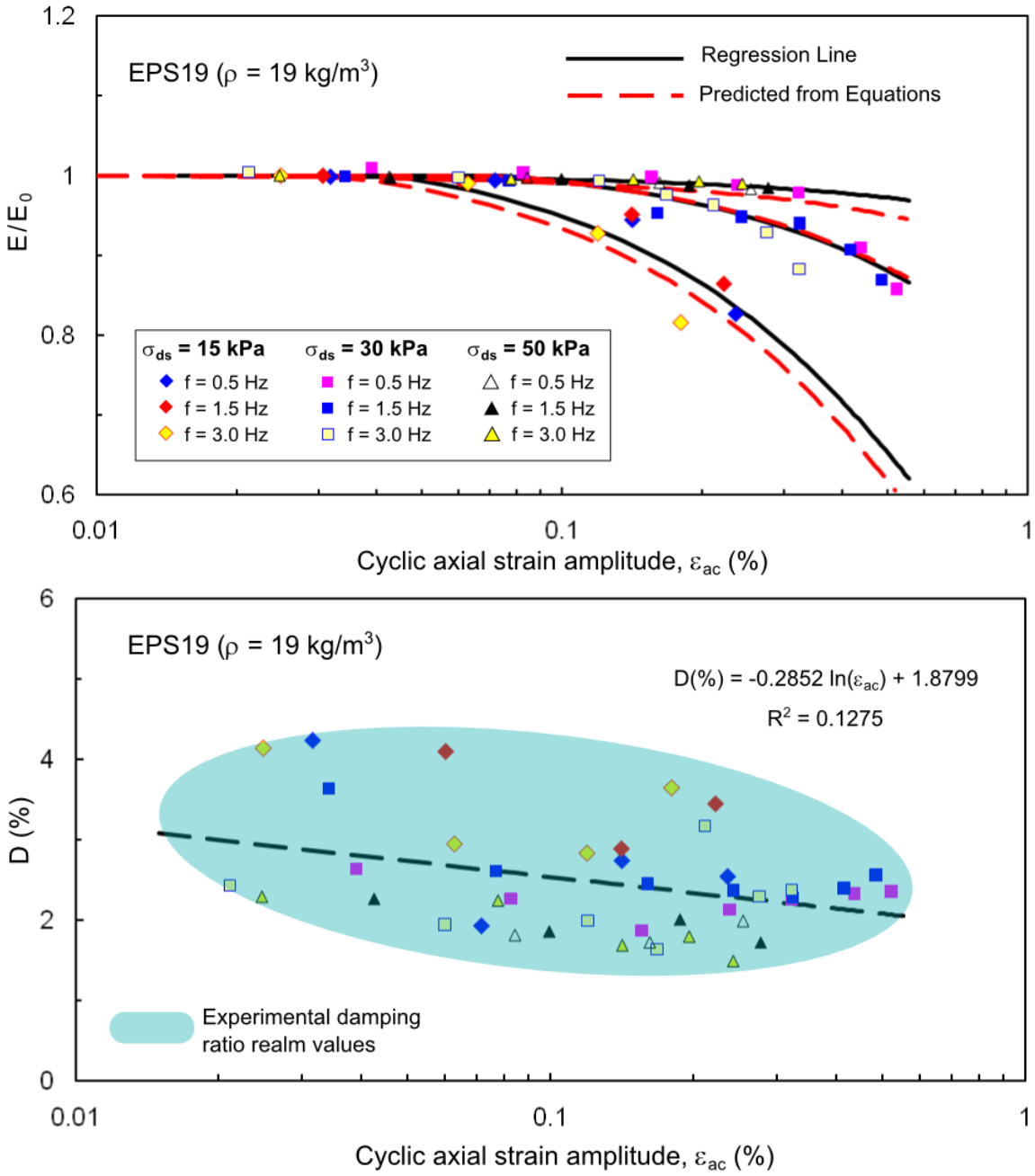

Figure 13: The normalized Young's modulus (E/E_0) and damping ratio (D) of EPS19 geofoam vs cyclic axial strain amplitude (ε_{ac}) for various static deviator stress (σ_{ds}) and loading frequencies (f).

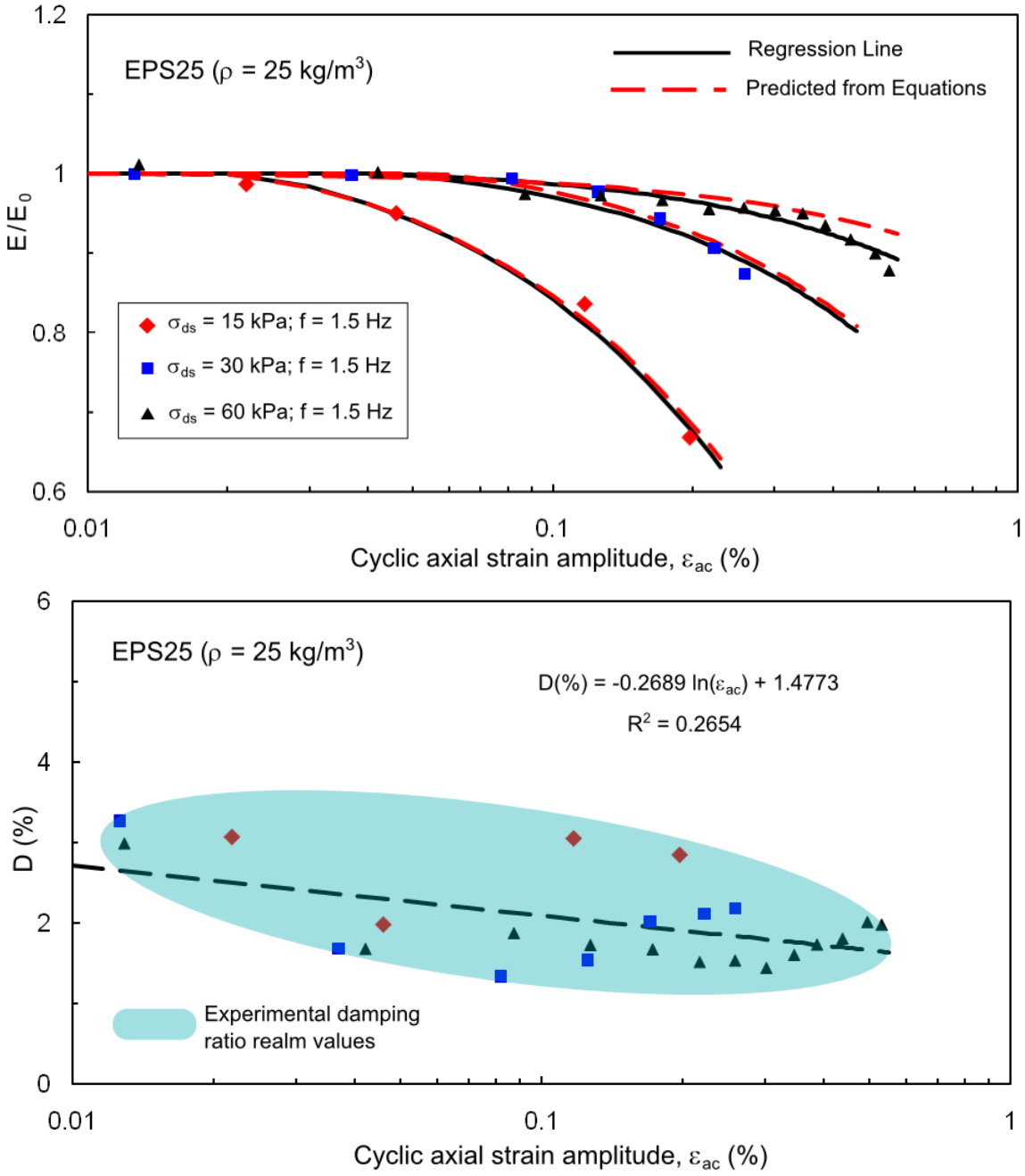

Figure 14: The normalized Young's modulus (E/E_0) and damping ratio (D) of EPS15 geofoam vs cyclic axial strain amplitude (ε_{ac}) for various static deviator stress (σ_{ds}) and loading frequencies (f).

For further evidence of this trend of decreasing D, comparing the hysteresis loops in Figure 15 shows a breadth compression, W_d dissipated energy from Figure 11, for cyclic deviator stress increase related to the stored energy W_s, also from Figure 11. From the density comparison tests the range of D was from 1.3-4.3% with an average of 2.3%. The slight decrease of D may be related to EPS geofoam fabric alteration becoming resisting to absorbing energy as strains increase. This alteration may also be related to the material creep and its stiffening effect, although less apparent regarding damping ratio than the static deviator stress results.

Visco-elasto-plastic behavior

The results from the visco-elasto-plastic response of EPS geofoam tests have similar hysteresis loops, as discussed for a viscoelastic response; however, because there is no closed hysteresis loop, plastic axial strain (ε_{ap}) accumulates with each cycle. As shown in Figure 16, the accumulated plastic axial strain can be defined as the walking distance in terms of axial strain of the loading loops along the horizontal axis for the applied number of loading cycles (N). It is apparent that the larger the cyclic deviator stress amplitude, the larger the plastic axial strains for the same number of applied loading cycles.

Figure 17 shows the relationship of plastic axial strain compared to the applied number of stress cycles. For EPS15, undergoing σ_{ds} = 35 kPa and cyclic frequency of 1.5 Hz after 300 cycles of $\Delta\sigma_{dc}$ = 18 kPa the specimen reaches 0.54% of permanent axial strain. This is being much smaller than that for $\Delta\sigma_{dc}$ = 27 kPa which produces a value of ε_{ap} = 2.31% for the same number of loading cycles. The slower increase in ε_{ap} with increasing number of cycles suggests a larger plastic strain response during the initial

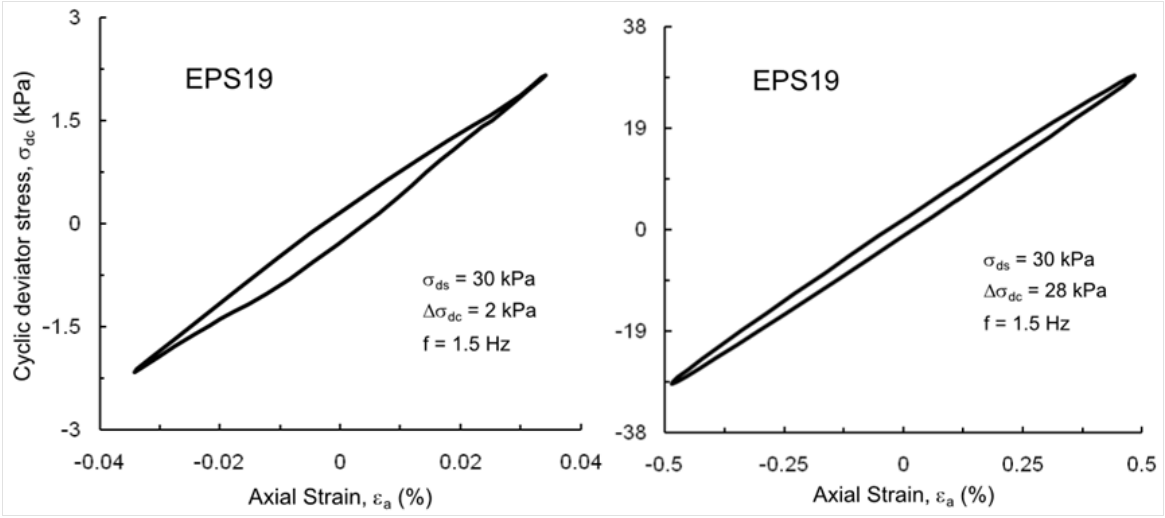

Figure 15: Comparative stress strain response of EPS19 geofoam with different cyclic deviator stress amplitudes ($\Delta\sigma_{dc}$) but with same static deviator stress (σ_{ds}) values.

loading cycles, which gradually attenuates as the number of loading cycles progress. Over time the plastic axial strain and loading cycles achieve a constant slope of the ε_{ap} – N relationship after a certain number of cycles.

Plastic yield onset under cyclic loading

In anticipation of the material application an expectation of the material behavior, concerning yield strength, needs to be evaluated. An evaluation of the yield strength was performed of each density using rapid monotonic triaxial loading. As shown in Figures 18-20 the results of the monotonic loading uniaxial tests using a strain rate of 10%/minute (i.e., $(\sigma_{dm})_{yield}$)) the results indicate yielding under cyclic test under smaller cyclic deviator stress, compared to the rapid monotonic loading tests. It can be concluded that using yield strengths from rapid monotonic loading to predict the response of geofoam under cyclic loading may result in an over estimate of the total dynamic deviator stress required to trigger plastic strains in EPS geofoam.

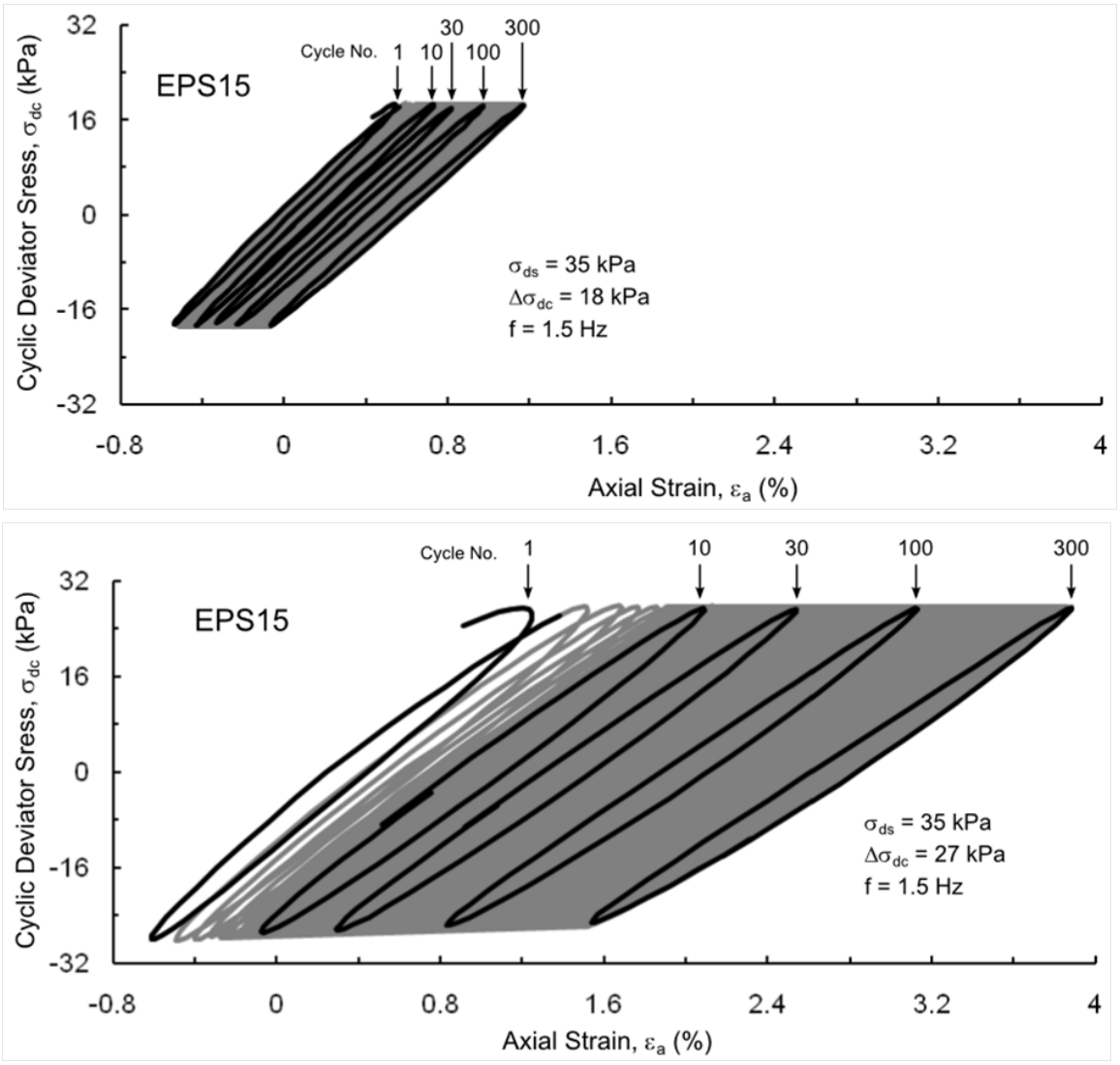

Figure 16: EPS15 visco-elasto-plastic stress-strain response with the same static deviator stress (σ_{ds}) but different cyclic deviator stress amplitudes ($\Delta\sigma_{dc}$).

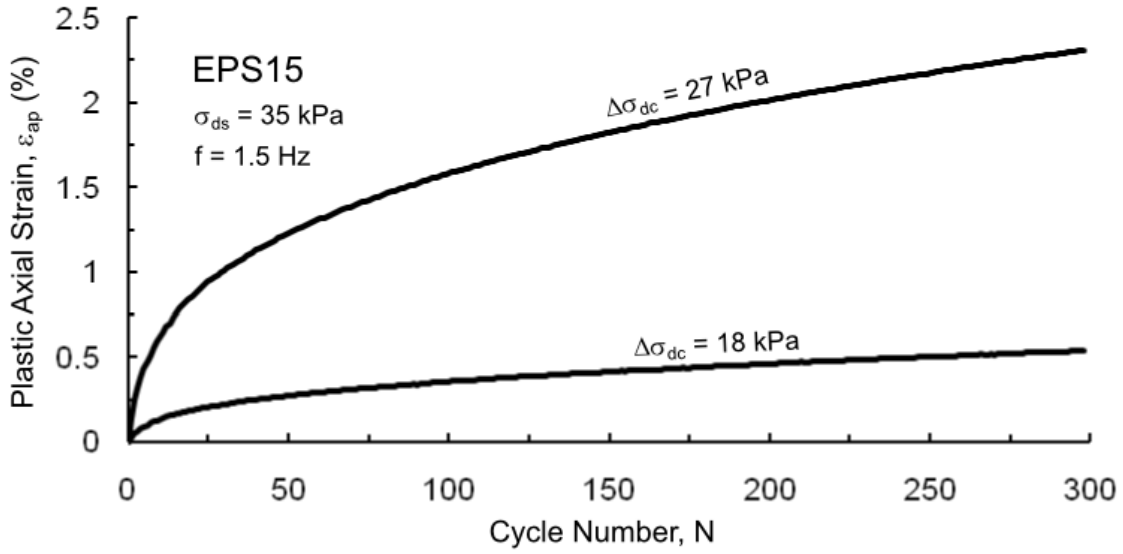

Figure 17: Relationship between ε_{ap} and loading cycle number for different cyclic deviator stress amplitudes ($\Delta\sigma_{dc}$).

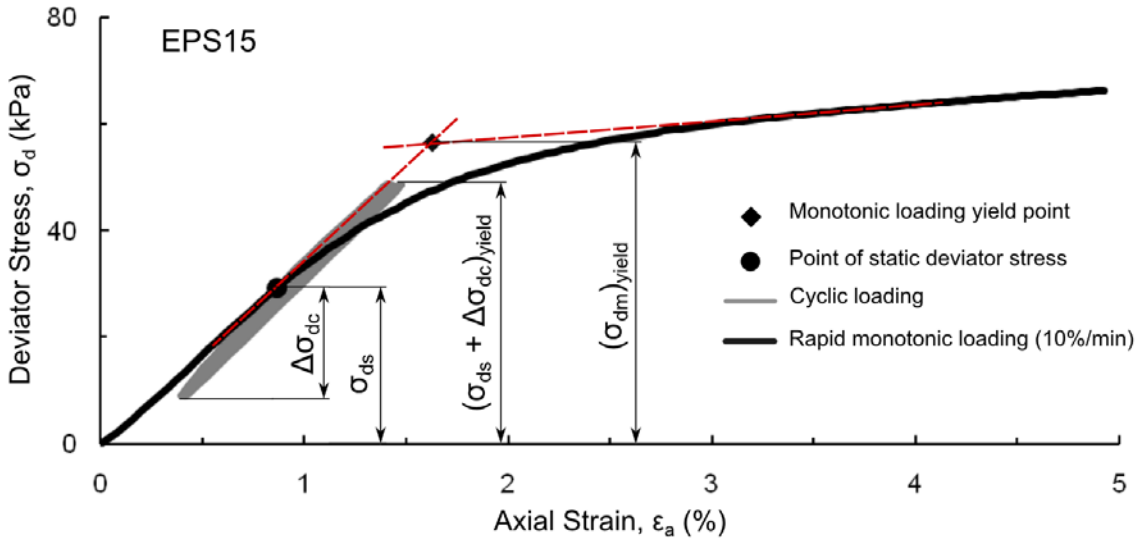

Figure 18: An illustration of EPS15 yield point evaluation through rapid monotonic loading uniaxial test. A comparative hysteresis loop of non yielding cyclic test with associated static deviator stress point.

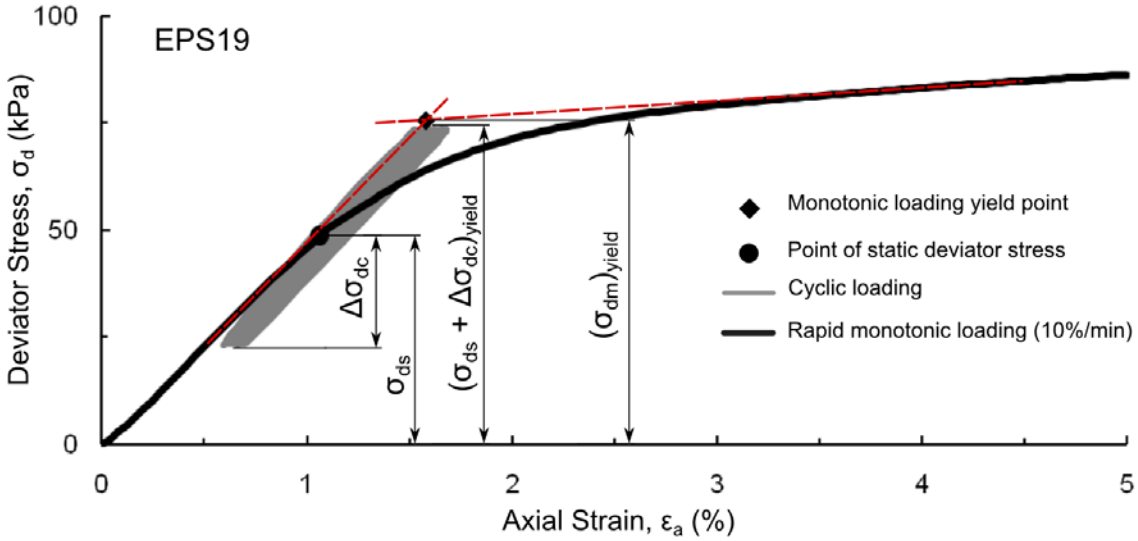

Figure 19: An illustration of EPS19 yield point evaluation through rapid monotonic loading uniaxial test. A comparative hysteresis loop of non yielding cyclic test with associated static deviator stress point.

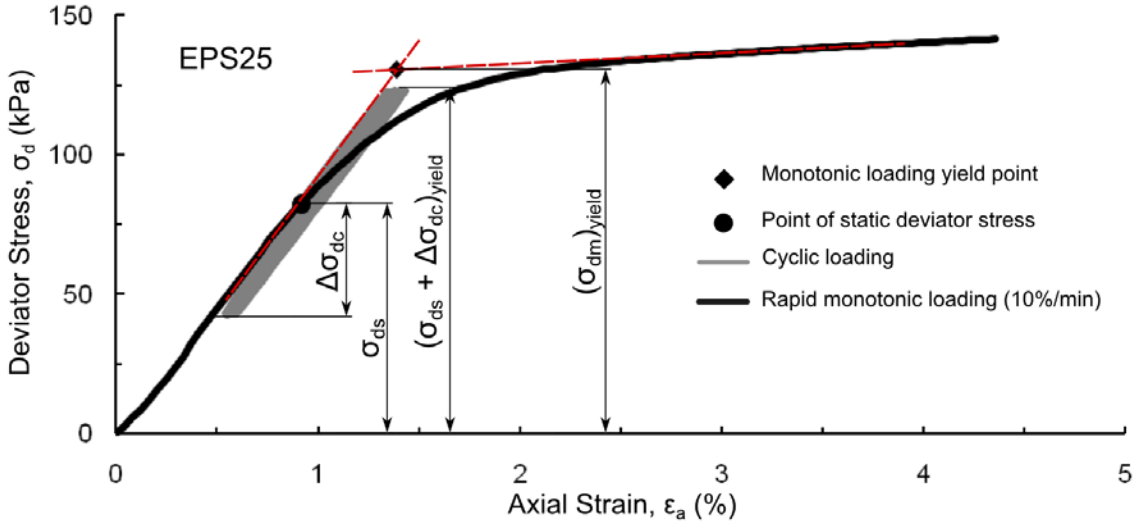

Figure 20: An illustration of EPS25 yield point evaluation through rapid monotonic loading uniaxial test. A comparative hysteresis loop of non yielding cyclic test with associated static deviator stress point.

Initial Young's modulus of EPS geofoam

The initial Young's modulus (E_0) was derived as the Young's modulus (E) value related to a cyclic axial strain amplitude equaling 0.01% (ε_{ac} = 0.01%) from a regression analysis of each test series of cyclic uniaxial test with a specific loading frequency, static deviator stress and geofoam density. Figure 21 illustrates the relationship between E_0 and tested densities. Resulting in a regression line equation, where the density (ρ) is in kg/m^3.

$$E_0 = 59.93\rho^2 - 1622.8\rho + 15602 \quad (4)$$

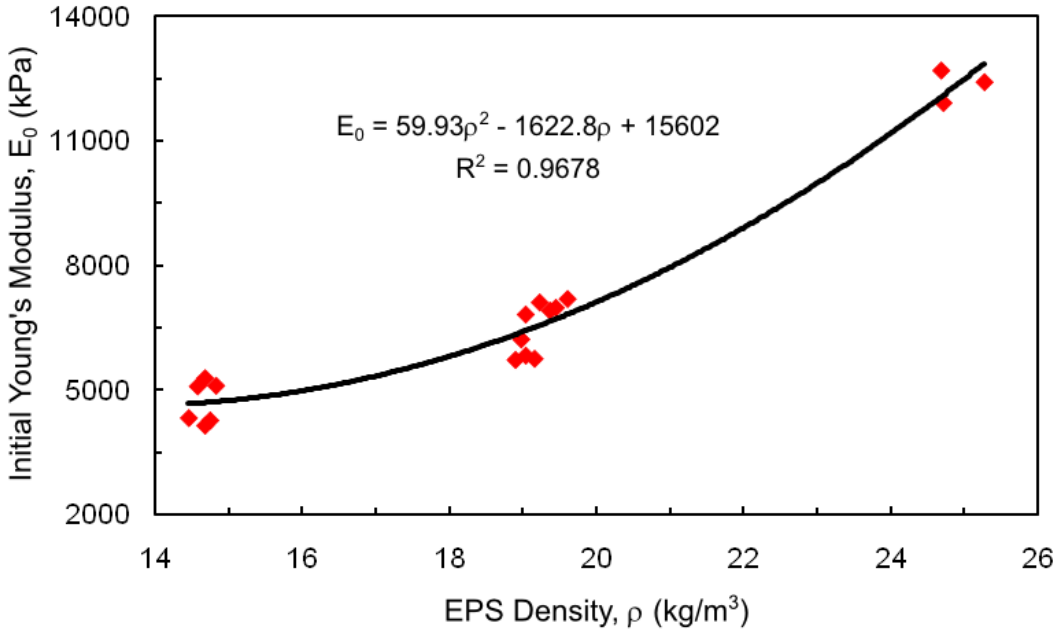

Figure 21: Initial Young's modulus and EPS densities 15, 19 and 25 kg/m^3 from cyclic tests.

FREQUENCY EFFECTS

As described in the experimental setup section, frequencies of 0.5, 1.5 and 3.0 Hz were evaluated. Figure 22 illustrates no difference of these frequencies in the hysteresis loops. Therefore, frequency has no significant impact on the shape of the hysteresis loop for geofoam in viscoelastic stress-strain domain for the range of frequencies explored in this test program.

In the case of plastic strains and the effect of loading frequencies have on EPS geofoam; the visco-elasto-plastic response shows some differences when compared to the viscoelastic response. Figure 23 shows the behavior of EPS19 during various loading frequencies comparing two tests, where both are under the same static deviator stress (σ_{ds} = 50 kPa). One test uses a smaller cyclic deviator stress ($\Delta\sigma_{dc}$ = 25 kPa) while the other test uses a higher cyclic deviator stress ($\Delta\sigma_{dc}$ = 35 kPa). In both cases the lower loading frequency (f = 0.5 Hz) is exhibiting a larger plastic strain with applied cyclic number than the greater loading frequency (f = 1.5 Hz).

The visco-elasto-plastic response provides some insight to the viscous nature of EPS geofoam. The more time for abortion of energy, as manifest by slower cycling, the more plastic deformation occurs for the same cyclic deviatoric stress amplitude. However, as illustrated by the viscoelastic response, the damping energy effect of geofoam will not increase with a decrease in frequency. Therefore, energy will be better absorbed in the visco-elasto-plastic response of geofoam.

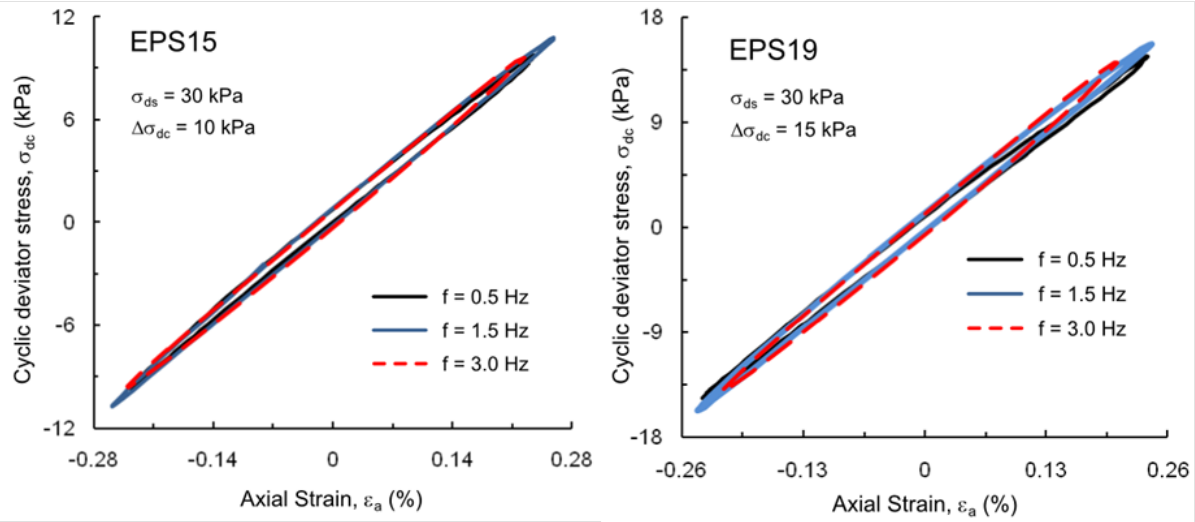

Figure 22: Hysteresis loops of frequencies varying from 0.5, 1.5 and 3.0 Hz for a uniaxial viscoelastic response of EPS15 and EPS19 geofoam.

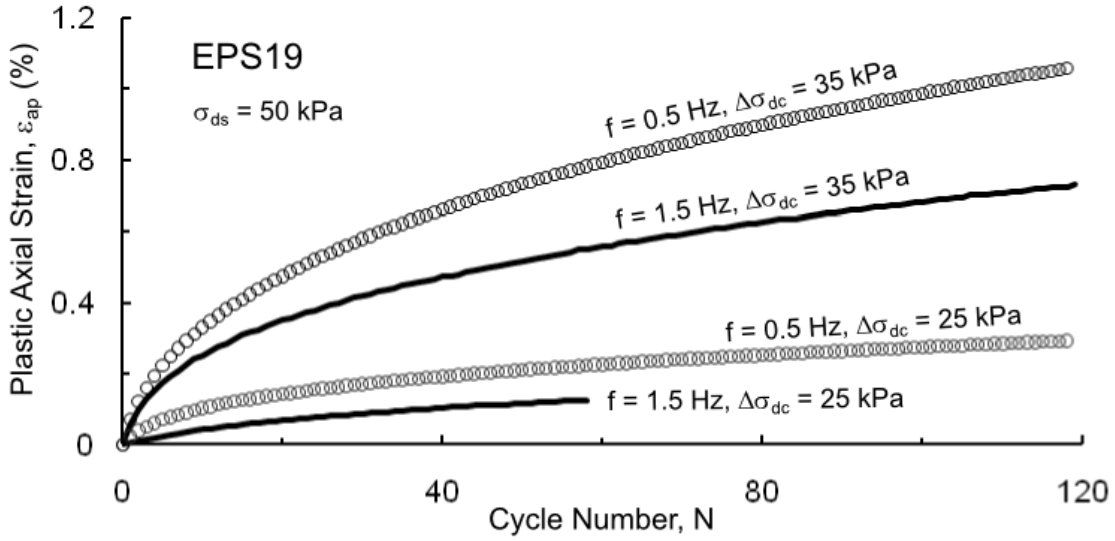

Figure 23: The visco-elasto-plastic response of EPS geofoam with the influence of loading frequencies (*f*) under different cyclic deviator stress amplitudes ($\Delta\sigma_{dc}$).

CONFINING STRESS EFFECT

The influence of confining stress effect on EPS geofoam was investigated through triaxial stress-controlled cyclic tests. The test sets used a cyclic frequency of f = 1.5 Hz and were applied on a EPS19 cylinder sample of d = 100 mm and h:d = 2:1. The tests consisted of a initial (static) isotropic stress state with the major (σ_{1s}) and minor (σ_{3s}) principal stress values equal to the confining stress level (σ_c) applied to the specimen prior to the cyclic loading phase of the test (i.e., $\sigma_{1s} = \sigma_{3s} = \sigma_c$). Values of confining stress (σ_c) levels used in the test were 15, 30 and 50 kPa. Whereas the major and minor principal stresses in a cyclic uniaxial test are $\sigma_c = 0$ and $\sigma_{1s} = \sigma_{ds}$, respectively.

Results of the triaxial test, shown in Figure 24, illustrates the dynamic viscoelastic properties of geofoam when measured for various confining stresses (i.e., $\sigma_c > 0$). The confining stress does not have any apparent influence on the normalized Young's modulus (E/E_0). The E/E_0 values from this investigation are narrowly scattered and are within the range of published modulus degradation relationships (Athanasopoulos et al., 1999, Athanasopoulos et al., 2007; Ossa and Romo, 2008). However, the static confining stress (σ_c) has significant effect on the damping ratio of EPS geofoam. The damping ratio shows a significant increase as the confining stress increases. For example, cyclic axial strain amplitude ε_{ac} = 0.33% the damping ratio (D) increases from 2.3% for $\sigma_c = 0$ to 18% for σ_c = 30 kPa, and reaches about 25% for σ_c = 50 kPa. This behavior is further

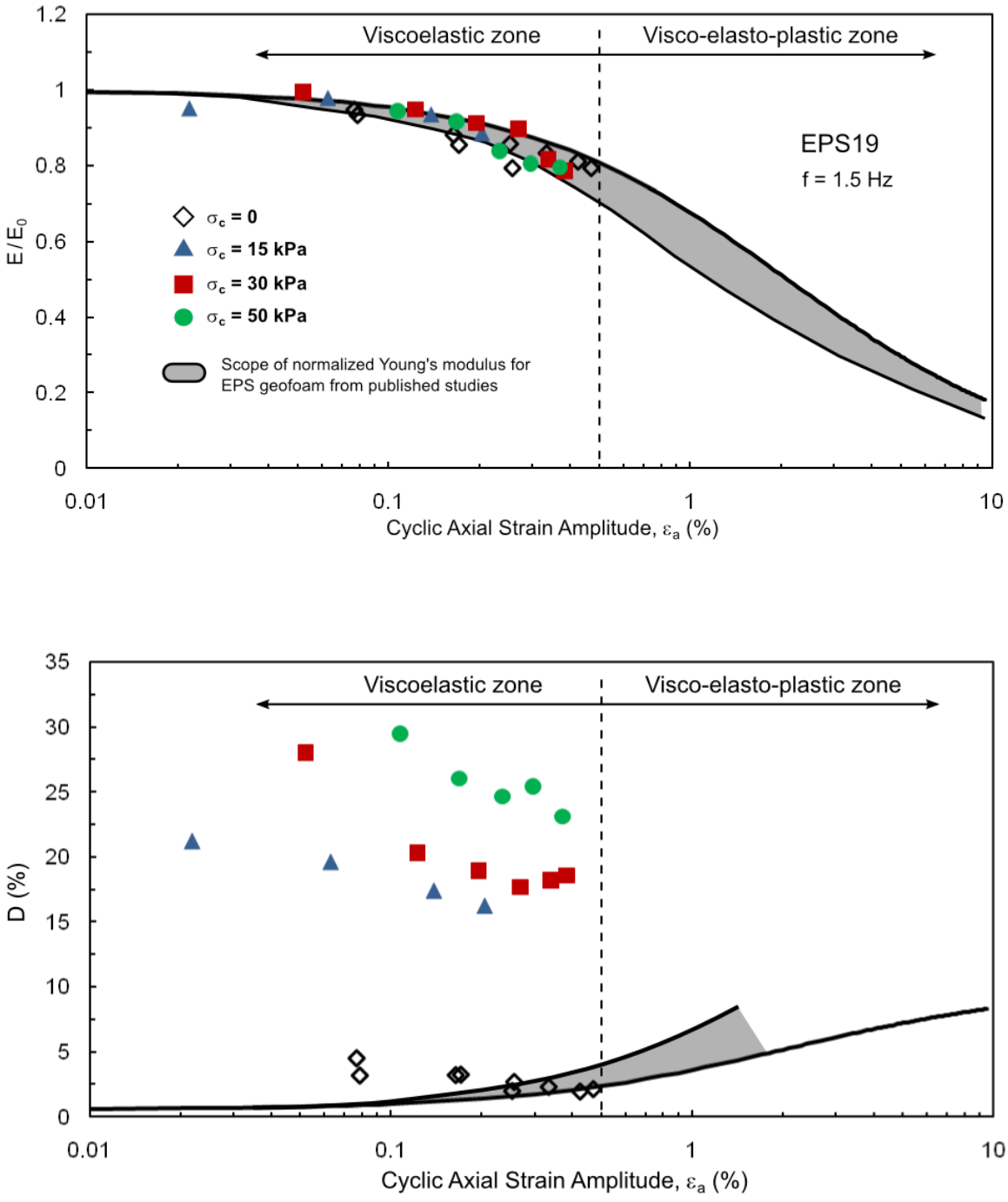

Figure 24: Various static confining stresses plot of normalized Young's modulus and damping ratio of EPS geofoam vs cyclic axial strain amplitude.

illustrated in Figure 25 by the increased breadth (i.e., area) of the hysteresis loop, which confining static stress (σ_c = 30 kPa) is compared to the response of an unconfined sample (σ_c = 0). Both samples are subjected to the same major principal stress (σ_{1s} = 30 kPa) and similar deviator stress amplitudes ($\Delta\sigma_{dc}$ = 20 kPa). The damping ratio results indicate a slight to moderate decrease with an increase in cyclic axial strain amplitude (Figure 24) and in general a *D* value when compared to those published literature for stain amplitudes up to 0.5%.

The static confining stress (σ_c) effect under cyclic loading on plastic yielding geofoam was also investigated. As illustrated by Figure 27, the response of confined (i.e., σ_c = 50 kPa) and unconfined (i.e., σ_c = 0) cyclic stress-strain tests are imposed the same static major principal stress (i.e., σ_{1s} = 50 kPa) as well as similar cyclic deviator stress amplitudes (i.e., $\Delta\sigma_{dc}$ = 37). The resulting horizontal walking distance of the unloading-reloading loop for the same number of loading cycles is much greater in the unconfined (i.e., σ_c = 0) than in the confined (i.e., σ_c = 50 kPa) test. Accordingly, the unconfined specimen of geofoam exhibits a larger plastic strain increase during one cycle of loading than compared to the confined geofoam sample. Figure 26 further illustrates the behavior difference showing the accumulated plastic axial strain (ε_{ap}) associated with the number of loading cycles for the cyclic uniaxial and triaxial test shown in Figure 27. The unconfined specimen accumulated permanent axial strain of ε_{ap} 2.4% from a 300 loading cycles applied during the test, this is substantially larger than the confined axial strain of ε_{ap} = 0.16% resulting from the confined geofoam sample. Likewise, geofoam demonstrated a faster attenuation in plastic strain increments under static confining stress compared to the unconfined test (Figure 26).

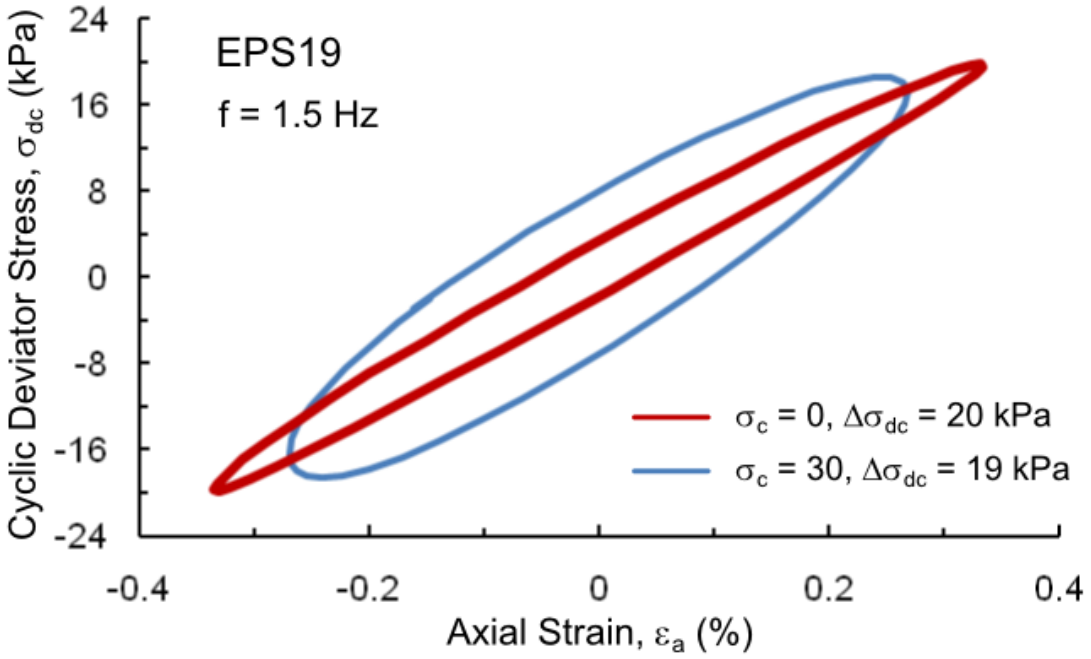

Figure 25: Stress-strain viscoelastic response of unconfined ($\sigma_c = 0$) and confined ($\sigma_c = 30$ kPa) EPS geofoam in cyclic uniaxial and triaxial compression tests.

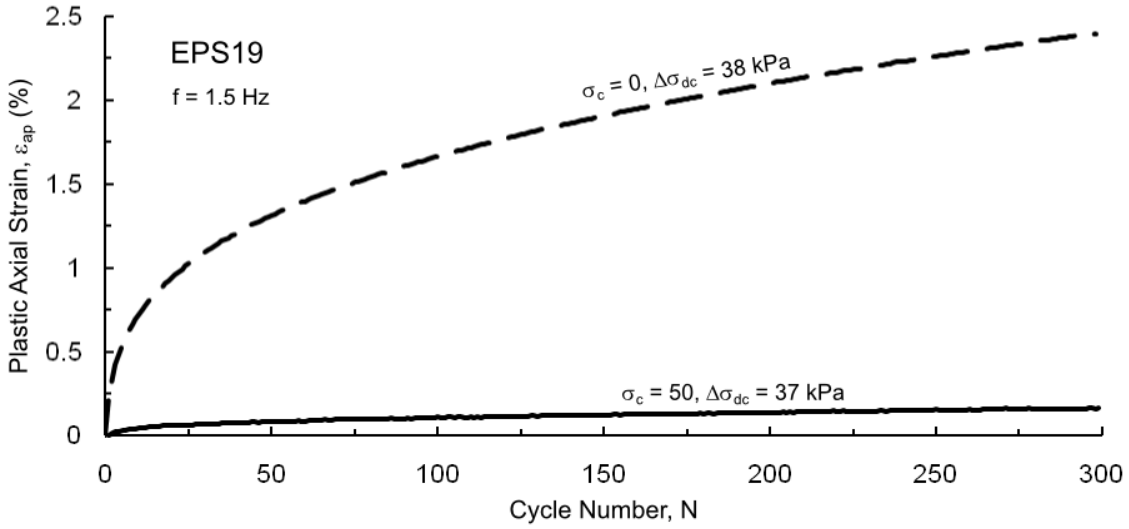

Figure 26: Cyclic uniaxial and triaxial accumulated plastic axial strain in relation to the number of loading cycles for unconfined ($\sigma_c = 0$) and confined ($\sigma_c = 50$ kPa) compression tests.

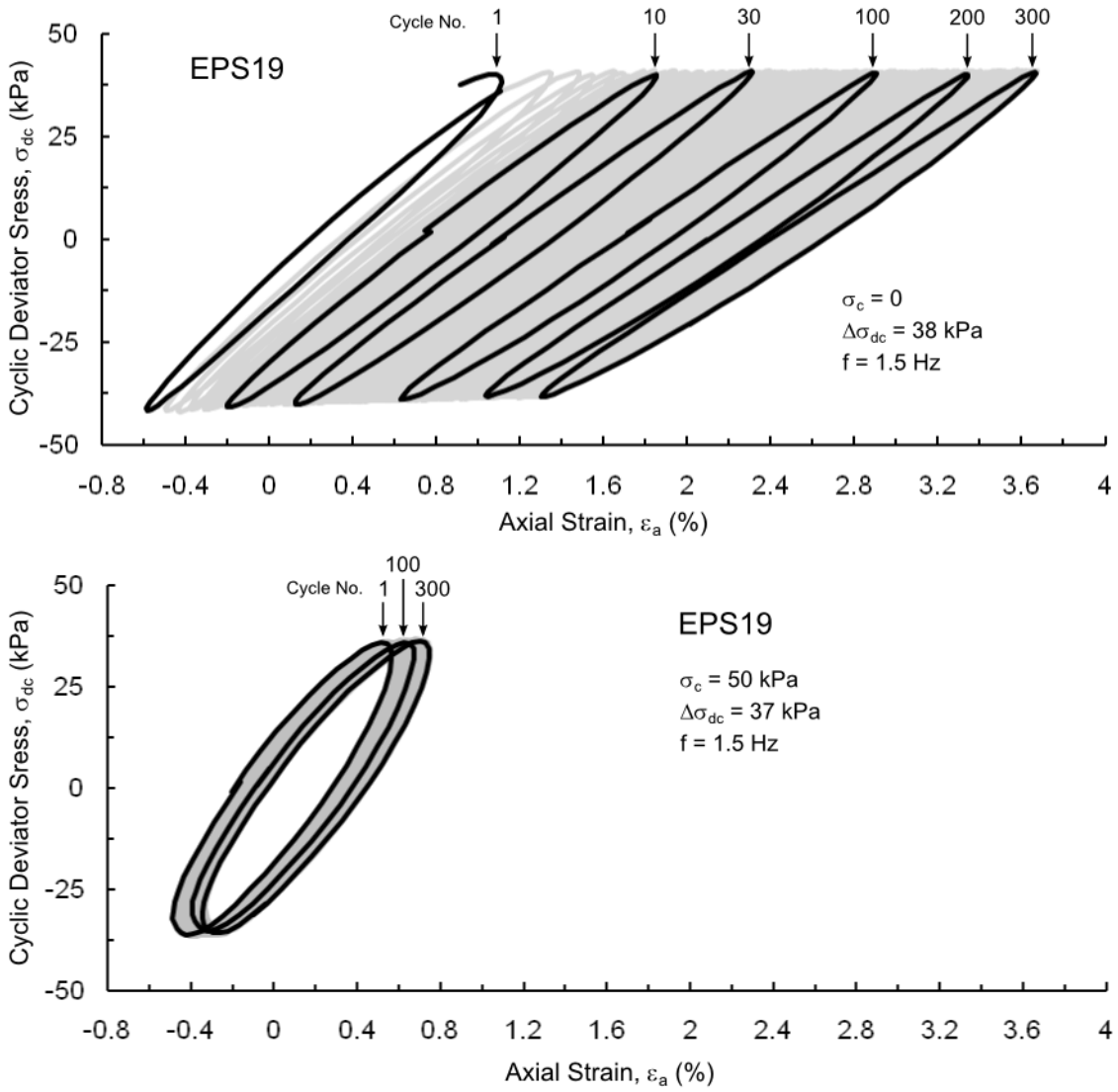

Figure 27: Visco-elasto-plastic stress-strain response of unconfined ($\sigma_c = 0$) and confined ($\sigma_c = 50$ kPa) cyclic uniaxial and triaxial compression tests of EPS19 geofoam.

CONCLUSIONS

Dynamic stress-strain analysis was conducted on specimens of EPS geofoam using uniaxial and triaxial cyclic compression tests. The effect of initial (static) deviator stress on the cyclic stress-strain behavior of geofoam was evaluated. The effect of loading frequency and cyclic deviator stress amplitudes as well as the confining stress effect of geofoam dynamic response were investigated. Some results of the tests yielded cases of no significant effect; such are the cases of frequency effect under viscoelastic response with no change in hysteresis loops; and the confining stress effect with the normalized Young's modulus (E/E_0), where the resulting narrow scatter plot was not influenced by the confining stress compared to unconfined stress. However, the effect of creep strain may have an influence on E due to stiffening to the material. The creep influence needs further evaluation to determine the type of influence on E.

On the other hand, when there was influential effect on the samples of EPS geofoam, the effect was substantial. Such effects are observation of energy absorption from the frequency variation effects, as well as the damping ratio (D) effect in addition to the plastic axial strains, being increased and more restricted due to the confining stress effect on geofoam.

CONCLUSION IMPACTS

The results of dynamic stress-strain analysis conducted on specimens EPS geofoam using uniaxial and triaxial cyclic compression tests have direct implications for the application of EPS geofoam in practical geotechnical problems. Based on the result of these tests, expected behavior of geofoam in a confined environment, should be reevaluated from the unconfined design. The resulting behavior differences are primarily beneficial for design performance application of EPS geofoam. Because of these results, there can be an expansion of application possibilities of geofoam.

As with the development of geofoam as a soil replacement, further development of geofoam as a seismic buffer will allow for higher confidence in structure designs and growth in geotextile development. Because of these results, new applications will primarily affect underground surface designs allowing for seismically prone environments to be considered. As further analysis is performed based on these results a better understanding of geofoam behavior associated with frequency effects and confining pressures will provide alterations of standards for geofoam implementation.

As discussed earlier, the apparent stiffening effect related to material creep caused by the static deviator stress prior to the cyclic phase of the test, will need further analysis to examine how influential this phenomenon is in geofoam implementation. Current designs do not fully take into account the stiffening behavior and additional analysis will

assist in best practice relating to the behavior and provide expectations for future designs related to applied static deviator stress on geofoam.

The overall conclusions of this study have provided an initial understanding of behavior of EPS geofoam under parameters which can be expected in practical applications for the material. Further analysis will complement the current knowledge on behavior of geofoam as a soil replacement and seismic buffer material.

APPENDIX: EXCEL FILES

See Supplemental Files

REFERENCES

Athanasopoulos, G.A., Nikolopoulou, C.P., Xenaki, V.C., and Stathopoulou, V.D., 2007, Reducing the seismic earth pressure on retaining walls by EPS geofoam buffers - numerical parametric study, Proceedings of the Geosynthetics Conference, Washington, DC, p. 16-19.

Athansopoulos, G.A., Pelekis, P.C., and Xenaki, V.C., 1999, Dynamic Properties of EPS Geofoam: An Experimental Investigation, Geosynthetics International 6, p. 171-194.

Barrett, J.C., Valsangkar, A.J., 2008, Effectiveness of connectors in geofoam block construction. Geotextiles and Geomembranes 27, p. 211–216.

Bathurst, R.J., Keshavarz, A., Zarnani, S., Take, W.A., 2006, A simple displacement model for response analysis of EPS geofoam seismic buffers, Soil Dynamics and Earthquake Engineering 27, p. 344–353.

Bathurst, R.J., Zarnani, S., Gaskin, A., 2006, Shaking table testing of geofoam seismic buffers, Soil Dynamics and Earthquake Engineering 27, p. 324–332.

Chun, B.S., Lim, H., Sagong, H.-S., Kim, K., 2004, Development of a hyperbolic constitutive model for expanded polystyrene (EPS) geofoam under triaxial compression tests, Geotextiles and Geomembranes 22, p. 223–237.

Choo, Y.W., Abdoun, T.H., O'Rourke, M.J., Ha, D., 2007, Remediation for buried pipeline systems under permanent ground deformation, Soil Dynamics and Earthquake Engineering 27, p. 1043–1055.

Elragi, A., Negussey, D., Kyanka, G., 2000, Sample Size Effects on the Behavior of EPS Geofoam, Soft Ground Technology, Proceedings of the Soft Ground Technology Conference, pp 280-291.

EPS Geofoam 1996, 2nd International Conference, Tokyo, Japan, October 1996.

EPS Geofoam 2001, 3rd International Conference, Salt Lake City, Utah, USA, December 2001.

EPS Geofoam 2011, 4th International Conference, Oslo, Norway, June 2001.

Farnsworth, C.B., Bartlett, S.F., Negussey, D., Stuedlein, A.W., 2008, Rapid Construction and Settlement Behavior of Embankment Systems on Soft Foundation Soils, Journal of Geotechnical and Geoenvironmental Engineering, v. 134, n. 3, p. 289-301.

Frydenlund, T. E., Aabøe, R., 2001, Long Term Performance and Durability of EPS as a Lightweight Filling Material, EPS Geofoam 2001, 3rd International Conference, Salt Lake City, December, 2001, 14 p.

Hazarika, H., 2006, Stress–strain modeling of EPS geofoam for large-strain applications, Geotextiles and Geomembranes 24, p. 79–90.

Horvath, J.S., 1995, Geofoam Geosynthetic, Horvath Engineering. P.C., Scarsdale, NY, USA, 217 p.

Horvath, J.S., 1996, The Compressible Inclusion Function of EPS Geofoam: An Overview, Proceedings of the International Symposium on EPS Construction Method, Tokyo, Japan, p. 71-81.

Horvath, J.S., 1999, Status of ASCE Standard on Design and Construction of Frost Protected Shallow Foundations, Journal of Geotechnical and Geoenvironmental Engineering, p. 166-167.

Ikizler, B.S., Aytekin, M., Nas, E., 2007, Laboratory study of expanded polystyrene (EPS) geofoam used with expansive soils, Geotextiles and Geomembranes 26, p. 189–195.

Ikizler, S.B., Aytekin M., Vekli, M., Kocabas, F., 2009, Prediction of swelling pressures of expansive soils using artificial neural networks, Advances in Engineering Software 41, p. 647–655.

Leo, C.J., Kumruzzaman, M, Wong, H., Yin, J.H, 2007, Behavior of EPS geofoam in true triaxial compression tests, Geotextiles and Geomembranes 26, p. 175–180.

Lin, L-K, Chen, L-H, Chen, R.H.L., 2010, Evaluation of Geofoam as a Geotechnical Construction Material, Journal of Materials in Civil Engineering, v. 22, n. 2, p. 160-170.

Liu, H.-l., Deng, A., Chub, J., 2006, Effect of different mixing ratios of polystyrene pre-puff beads and cement on the mechanical behaviour of lightweight fill, Geotextiles and Geomembranes 24, p. 331–338.

Murillo, C., Thorel, L., Caicedo, B., 2009, Ground vibration isolation with geofoam barriers: Centrifuge modeling, Geotextiles and Geomembranes 27, p. 423–434.

Negussey, D., 1997, Properties & Applications of geofoam, Society of the Plastics Industry, Inc., 22 p.

Newman, M.P., Bartlett, S.F., Lawton, E.C., 2010, Numerical Modeling of Geofoam Embankments, Journal of Geotechnical and Geoenvironmental Engineering, v. 136, n. 2, p. 290-298.

Osborn, P., 2004, Geofoam offers positive solutions: Foam plastic proven to be beneficial on some of the largest projects in the country. Roads & Bridges, September, p 64.

Ossa, A., and Romo, M.P., 2008, A model for EPS dynamic shear modulus and damping ratio, Proceedings of First Pan American Geosynthetics Conference and Exhibition, p. 894-901.

Stark, T., Arellano, D., Horvath, J., and Leshchinsky, D., 2004, NCHRP Report 529: Guideline and Recommended Standard for Geofoam Applications in Highway Embankments, Transportation Research Board, Washington, D.C., 51 p.

Trandafir, A.C, Bartlett, S.F., Lingwall, B.N., 2010, Behavior of EPS geofoam in stress-controlled cyclic uniaxial tests, Geotextiles and Geomembranes 28, p. 514–524.

Trandafir, A.C., Moyles, J.F., Erickson, B.A., in press, Finite-element Analysis of Lateral Pressures on Rigid Non-yielding Retaining Walls with EPS Geofoam Inclusion.

Trandafir, A.C., Erickson, B.A., Moyles, J.F., Bartlett, S.F., in press, Confining Stress Effects on the Stress-strain Response of EPS Geofoam in Cyclic Triaxial Tests.

Unknown, 2009, Rich foam: Fill material has a lot to offer, Roads & Bridges, June, p. 59.

Wang, J.G., Sun, W., Anand S., 2008, Numerical investigation on active isolation of ground shock by soft porous layers, Journal of Sound and Vibration 321, p. 492–509.

Wang, Z.-L., Lia, Y.-C., Wang, J.G., 2006, Numerical analysis of attenuation effect of EPS geofoam on stress-waves in civil defense engineering, Geotextiles and Geomembranes 24, p. 265–273.

Wong, H., Leo, C.J., 2006, A simple elastoplastic hardening constitutive model for EPS geofoam, Geotextiles and Geomembranes 24, p. 299–310.

Zarnani, S., Bathurst, R.J., 2008, Influence of constitutive model on numerical simulation of EPS seismic buffer shaking table tests, Geotextiles and Geomembranes 27, p. 308–312.

Zarnani, S., Bathurst, R.J., 2008, Numerical modeling of EPS seismic buffer shaking table tests, Geotextiles and Geomembranes 26, p. 371–383.

Zarnani, S., Bathurst, R.J., 2009, Numerical parametric study of expanded polystyrene (EPS) geofoam seismic buffers, Canadian Geotechnical Journal, v. 46, p. 318-338.